



# Effect of lignin on the thermal stability of cellulose nanofibrils produced from bagasse pulp

Ni Zhang · Peng Tao · Yanxv Lu · Shuangxi Nie

Received: 5 April 2019 / Accepted: 1 August 2019 / Published online: 3 August 2019  
© Springer Nature B.V. 2019

**Abstract** In this work, the effects of lignin on the thermal stability of bagasse cellulose nanofibrils (CNFs) were investigated. The CNFs were prepared with different lignin content bagasse pulp using ultrafine grinding combined with high-pressure homogenization. Scanning electron microscopy, Fourier transform infrared spectroscopy, X-ray diffraction and thermogravimetric analysis were used to study the influence mechanisms of lignin content on the thermal stability of the CNFs. The thermal stability of cellulose was tested by thermogravimetric analyzer at different heating rates, and the activation energy of bagasse cellulose nanofibrils was calculated by Flynn-Wall-Ozawa method. The results showed that the average width of CNFs prepared by the mechanical method was approximately 20 nm. The higher the

lignin contents in the CNFs, the lower the crystallinity and the better the thermal stability. The thermal decomposition activation energy of CNF fluctuates with the change of conversion rate. Under the same conversion rate, the higher the lignin contents in the CNFs, the larger the activation energy value. The average activation energies of NO-LCNF, L-LCNF, ML-LCNF, MH-LCNF, and H-LCNF were 208.14, 254.49, 412.95, 530.54 and 652.10 kJ/mol, respectively, during the conversion rate of 20% to 90%. The research results provide a theoretical basis for the pyrolysis mechanism and high value utilization of CNFs and have a profound impact on promoting the application and development of CNFs in emerging nanocomposites.

---

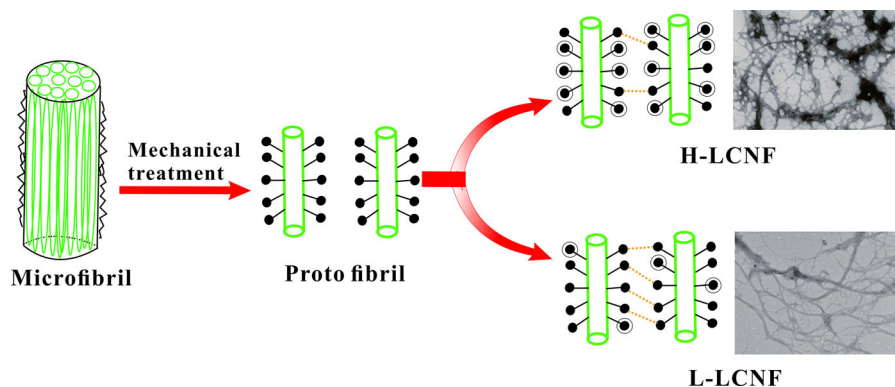
Peng Tao and Ni Zhang have contributed equally to this work.

---

N. Zhang · P. Tao · Y. Lu · S. Nie (✉)  
School of Light Industry and Food Engineering, Guangxi  
University, Nanning 530004, China  
e-mail: nieshuangxi@gxu.edu.cn

N. Zhang · P. Tao · Y. Lu · S. Nie  
Guangxi Key Laboratory of Clean Pulp & Papermaking  
and Pollution Control, Nanning 530004, China

## Graphic abstract



**Keywords** Lignin · Cellulose nanofibrils · Thermal stability · Crystallinity · Activation energy

## Introduction

With the emergence of global environmental changes and resource shortages, researchers are paying increased attention to sustainable and environmentally friendly materials (Dong et al. 2019; Nie et al. 2014; Wang et al. 2018; Yao et al. 2017; Zhang et al. 2019a). Cellulose nanofibrils (CNFs) are promising renewable nanomaterials due to their unique structure, excellent properties and natural abundance (Tao et al. 2019b; Tian et al. 2017; Zhang et al. 2019b). CNFs can be used to prepare green electronic products such as cellulose-based electronic flexible transistors, organic light-emitting diodes (OLEDs), printed antennas and radio frequency identification (RFID) devices, writable touch screens, and energy storage materials (Liao et al. 2018; Xing et al. 2019; Zhu et al. 2016). Thermal instability is a major problem with electronic devices based on biological materials. Because these materials typically have a lower melting temperature, these devices are susceptible to damage when annealed or sterilized as needed during device fabrication or operation (Wu et al. 2013). CNFs can be combined with other materials to produce a layered hybrid superlattice structure, which reduces the thermal conductivity of the material and provides a candidate material for thermoelectric energy harvesting (Tynell et al. 2014; Yoon et al. 2012).

The thermal stability of CNFs is related to many factors include plant fiber raw material components (hemicellulose, lignin, etc.) and CNF production methods (Nie et al. 2018a; Tao et al. 2019a; Zhang et al. 2018c). In plant fibers, hemicellulose and lignin act as fillers and binders to wrap a plurality of cellulose molecular chains together to form fiber bundles (Li et al. 2019; Lin et al. 2018; Nie et al. 2015; Penttila et al. 2013; Yao et al. 2015). Lignin is one of the three major components of plant fiber raw materials (Huang et al. 2019; Huang et al. 2016; Zhang et al. 2018a). It is a natural polymer compound with a three-dimensional network structure formed by a phenylpropane structure through a carbon-carbon bond and an ether bond (Kutscha and Gray 1970; Pei et al. 2016; Yu et al. 2018; Zhang et al. 2018b). Nair & Yan studied the effect of lignin on the thermal stability of CNFs. When the lignin content of CNFs was 21 wt.% and 5 wt.%, the initial degradation temperatures of CNFs were 306 °C and 278 °C, respectively, and the maximum degradation rates were 390 °C and 319 °C, respectively; thus, the presence of lignin significantly improved the thermal stability of CNFs (Nair and Yan 2015). The reason is that during the mechanical grinding process, lignin is wrapped on the surface of the fiber, which can reduce the generation of hydrogen bonds between the fibers. Thus, the fibers do not form a sheet connection, which reduces the heat receiving area and thereby improves the thermal stability. The thermal degradation of lignocellulosic fibers is a complex process involving a series of competitive and continuous reactions. Studies have shown that low residual lignin has no obvious effect on the thermal stability of CNFs (Alemdar and Sain 2008; Chen et al.

2011). Some researchers have attempted to produce CNF with high levels of lignin (20 wt.%), but they were unable to break the crosslinked lignin barrier and produce fibrils with a width of 1  $\mu\text{m}$  (Hoeger et al. 2013; Spence et al. 2010).

This work mainly studies the effect of lignin on the thermal stability of CNFs. Unbleached bagasse pulp and bleached bagasse pulp are mixed in different ratios, and CNFs are obtained and combined with ultrafine grinding and a high-pressure homogenization treatment. The thermal stability of CNFs was characterized by thermogravimetric analysis. The research results provide a theoretical basis for the pyrolysis mechanism and high-value utilization of CNFs and have far-reaching influence and important strategic significance for promoting the application and development of CNFs in emerging nanocomposites.

## Methods

### Chemicals and raw materials

Bagasse and bleached bagasse pulp boards were acquired from the Guangxi Guitang (Group) Co., Ltd. (Guangxi, China) and the bagasse pulp was pulped using the caustic soda method. The alkali content level was measured at 17.5%, the liquid ratio was measured at 1:3.5, the heating time was set to 45 min, and the maximum cooking temperature was set to 165  $^{\circ}\text{C}$  (which was maintained for 110 min). The unbleached pulp used had a Kappa number of 18.12 and a viscosity value of 1173.67 mg/L (Nie et al. 2018a). Sulfuric acid, acetone and starch were purchased from the Guangxi Nanning Boyu Co., Ltd. (Guangxi, China). All chemicals were of analytical grade.

### Experimental method

#### Preparation of CNF

A total of 1200 g of bagasse was immersed in a bucket containing distilled water for 5 min, and then ground 4 times with a disc grinder to obtain powdered bagasse. Appropriate amounts of bagasse powder and bleached bagasse slurry were mixed according to a mass ratio of 1:3, 1:1, or 3:1, and distilled water was added until the pulp concentration was 2% and the solution was

dissolved for 2 min. The pulp samples were first treated with a micro grinder (MKZA 10-15JIV, Japan). The disc rotation speed and clearance were adjusted to 1500 rpm and -100 rp, respectively, grinding for 2.5 hours. Thereafter, the milled pulp with a concentration of 0.8 wt.% was treated by a High-pressure homogenizer (M-110EH-30, Netherlands). The CNF sample was first homogenized with a pore size of 200  $\mu\text{m}$  at a pressure of 350 Bar for 5 times, and further homogenized with a pore size of 87  $\mu\text{m}$  at a pressure of 1500 Bar for 10 times (Nie et al. 2018b).

#### Determination of bagasse chemical composition

The chemical composition of the samples was analyzed using the Pulp and Paper Industry Technical Association (TAPPI) standard (TAPPI 1992). The hemicellulose in bagasse is composed of a xylan polymer, and the hemicellulose content was determined by the standard TAPPI method (method T 223 cm-84). The xylose content X was calculated as the formula (1). Each CNF sample was determined in triplicate and the average was calculated.

$$X = 1.38 \times \frac{V_1 - V_2}{m \times \frac{200}{500}} \cdot c \times \frac{24}{1000} \times 100\% \quad (1)$$

wherein  $V_1$  is the  $\text{Na}_2\text{S}_2\text{O}_3 \cdot 5\text{H}_2\text{O}$  solution consumed by the control test, mL;  $V_2$  is the  $\text{Na}_2\text{S}_2\text{O}_3 \cdot 5\text{H}_2\text{O}$  solution consumed by the sample, mL;  $c$  is the concentration of  $\text{Na}_2\text{S}_2\text{O}_3 \cdot 5\text{H}_2\text{O}$  solution, mol/L;  $m$  is the oven dry sample, g; 24 is the molar mass  $M$  ( $0.25 \text{ C}_5\text{H}_4\text{O}_2$ ) of furfural in the tetrabromination method, g/mol.

The Klason lignin content of the bagasse was measured by the standard TAPPI method (method T222 om-88). The lignin content L is calculated as the formula (2). Each CNF sample was determined in triplicate and the average was calculated.

$$L = \frac{m_1 - m_2}{m} \times 100 \quad (2)$$

wherein  $m_1$  is the mass of the acid-insoluble lignin after drying, g;  $m_2$  is the mass of ash in acid-insoluble lignin, g;  $m$  is the absolute dry mass of the sample, g.

### Preparation of CNF film

Forty-three grams of CNF suspension (concentration of 0.7 wt.%) was placed in a 500 mL glass beaker and thoroughly stirred by adding 400 mL of distilled water for 3 hours. The solution was poured into a sand core funnel placed with a 0.22  $\mu\text{m}$  PTFE membrane and vacuum-filtered to form a film. The dried film was placed in a polyethylene sealed bag for use by drying (50 °C) for 18 min using a Kaiser fast paper sheet former (HAAGE Sheet Former BB, Germany).

### TEM analysis

One gram of CNF suspension (concentration 0.7 wt.%) was placed into a 500 mL beaker, diluted to 0.008% with distilled water, sonicated for 30 min, and then stirred with a magnetic stirrer for 2 hours. Four Petri dishes containing filter paper were set up, and a copper mesh was placed on each filter paper with tweezers. The CNF suspension was dispersed and dropped onto a copper mesh to be beaded and dried at room temperature for 3 hours. After the drying was completed, 2% of phosphotungstic acid dyeing agent was dropped on the copper mesh. The dishes were left in the dark for 20 minutes, and then the excess dye was sucked off with filter paper. The CNF morphology was characterized by transmission electron microscopy (HT7700, Japan) at an operating voltage of 100 KV.

### Fourier transform infrared (FTIR) spectroscopy

Twenty grams of CNF suspension (concentration 0.7 wt.%) was placed into a dry Petri dish and dried at 105 °C. The dried sample was pulverized by a pulverizer, passed through a 60-mesh sieve, and formed into a film with potassium bromide. CNF characterization was performed using a Fourier transform infrared spectrometer (VERTEX 70, Germany) at a resolution of 0.4  $\text{cm}^{-1}$  and a wavenumber range of 500 to 4000  $\text{cm}^{-1}$ .

### X-ray diffraction (XRD) analysis

The CNF film was cut into  $2 \times 2 \text{ cm}^2$  size and attached to a fixed position of the glass sample plate. The crystallographic analysis was performed using a high-resolution X-ray diffractometer (SMARTLAB 3 KW, Japan). The scanning angle  $2\theta$  was in steps of 0.02

degrees, 2.5 seconds per step, from 5° to 40°. The CNF crystallinity index (CrI) was calculated according to the formula (3) (L. Segal et al. 1959):

$$\text{CrI} = 100 \times \frac{I_{200} - I_{am}}{I_{200}} \quad (3)$$

where  $I_{200}$  is a diffraction intensity of  $2\theta=22.5^\circ$ , which represents a crystallization zone;  $I_{am}$  is a diffraction intensity of  $2\theta=18.5^\circ$ , indicating an amorphous region.

### Thermogravimetric analysis (TGA)

Thermogravimetric analysis of CNF samples was performed using a synchronous thermal analyzer (STA 449F5, NETZSCH, Germany). 7 mg freeze-dried CNF sample was used in TGA, and all tests were carried out under a nitrogen atmosphere with a nitrogen flow rate of 40 mL/min. For the TG test, the heating rates were 5, 10, 15 and 20 °C/min, the temperature range was 30–600 °C.

### Calculation method of activation energy of each CNF sample

The Flynn-Wall-Ozawa (FWO) calculation method was employed to calculate the thermal decomposition kinetic parameters (Brown et al. 1980). The temperature dependent rate constant can be replaced by Arrhenius equation (Dhaundiyal et al. 2018), which gives us:

$$\frac{d\alpha}{dt} = A \exp\left(-\frac{E}{RT}\right) f(\alpha) \quad (4)$$

$$\alpha = \frac{w_0 - w}{w_0 - w_\infty} \quad (5)$$

Convert to the following equation:

$$\frac{d\alpha}{dT} = \frac{d\alpha}{dt} \frac{dt}{dT} = \frac{A}{\beta} \cdot \exp\left(-\frac{E}{RT}\right) f(\alpha) \quad (6)$$

Wherein  $a$  is the conversion rate, the value is 0 ~ 1;  $t$  is the time, min;  $A$  is the pre-factor,  $\text{min}^{-1}$ ;  $E$  is the activation energy, J/mol;  $R$  is the gas constant, the value is 8.314 J/(mol·K),  $T$  is the absolute temperature, K;  $f(a)$  is the reaction equation determined by the pyrolysis mechanism;  $w_0$  is the initial weight of the sample during the thermogravimetric analysis test, mg;  $w$  is the real-time weight of the sample during the test, mg;  $w_\infty$  is the final residual weight of the sample

after the reaction, mg;  $\beta$  is the rate of temperature rise, °C/min.

Integrating equation (6), it can be derived the following equation:

$$\log \beta = \log \left( A \frac{E}{Rg(x)} \right) - 2.315 - 0.4567 \frac{E}{RT} \quad (7)$$

With  $\log \beta$  as the ordinate and  $1/T$  as the abscissa, different heating rates can draw parallel lines parallel to each other at a fixed conversion rate. The slope of these lines is  $-0.4567 E/R$ .

## Results and discussion

### Characteristics of the produced cellulose nanofibrils

Table 1 shows the chemical composition of each CNF sample. The unbleached bagasse pulp has a low lignin content of 0.72% (No-LCNF) because ultrafine grinding causes a loss of components such as lignin in the pulp (Hassan et al. 2018). The content of lignin prepared from bagasse raw materials reached 22.81% (H-LCNF). The low lignin content of CNF (L-LCNF), the medium lignin content of CNF (ML-LCNF) and the higher lignin content of CNF (MH-LCNF) were prepared according to the 1:3, 1:1 and 3:1 ratios of bleached bagasse pulp and bagasse raw materials, respectively. Table 1 shows that the hemicellulose content of each CNF sample was basically unchanged and that hemicellulose has the same influence on CNFs.

Figure 1 shows a transmission electron micrograph of each CNF sample. It can be seen from Fig. 1 that each CNF was interwoven into a network. Approximately 50 single CNF fibers were selected for each image, and the average width was calculated with a nanomeasure. As shown in Table 1, each CNF had an average width of approximately 20 nm. The width of

each CNF sample showed a decreasing trend with increasing lignin content. Some scholars believe that the colloidal substance formed by lignin and hemicellulose tightly encloses the fibers, while lignin is linked to cellulose through strong covalent bonds. This colloidal substance and covalent bond blocks the microfibrillation process of fibers during mechanical grinding (Nair and Yan 2015). In addition, some scholars believe that the slurry will generate a large amount of mechanical free radicals during mechanical grinding, and a strong link between mechanical free radicals will hinder the microfibrillation of the fibers. Lignin contains a large amount of phenolic compounds, and phenolic compounds are antioxidants. When the lignin content in the pulp was high, a large amount of phenolic compounds undergo a radical reaction upon contact with mechanical radicals to form a covalent bond, thereby forming a very stable phenoxy radical, which can remove mechanical free radicals (as shown in Fig. 2) (Rojo et al. 2015; Solala et al. 2012). This will promote the microfibrillation of fibers, making the prepared CNF width smaller. In this study, the colloidal substances formed by lignin and the covalent bonds formed between the fibers interfere with the microfibrillation of the fibers, but the role of lignin was dominant in the removal of mechanical free radicals to promote fiber microfibrillation.

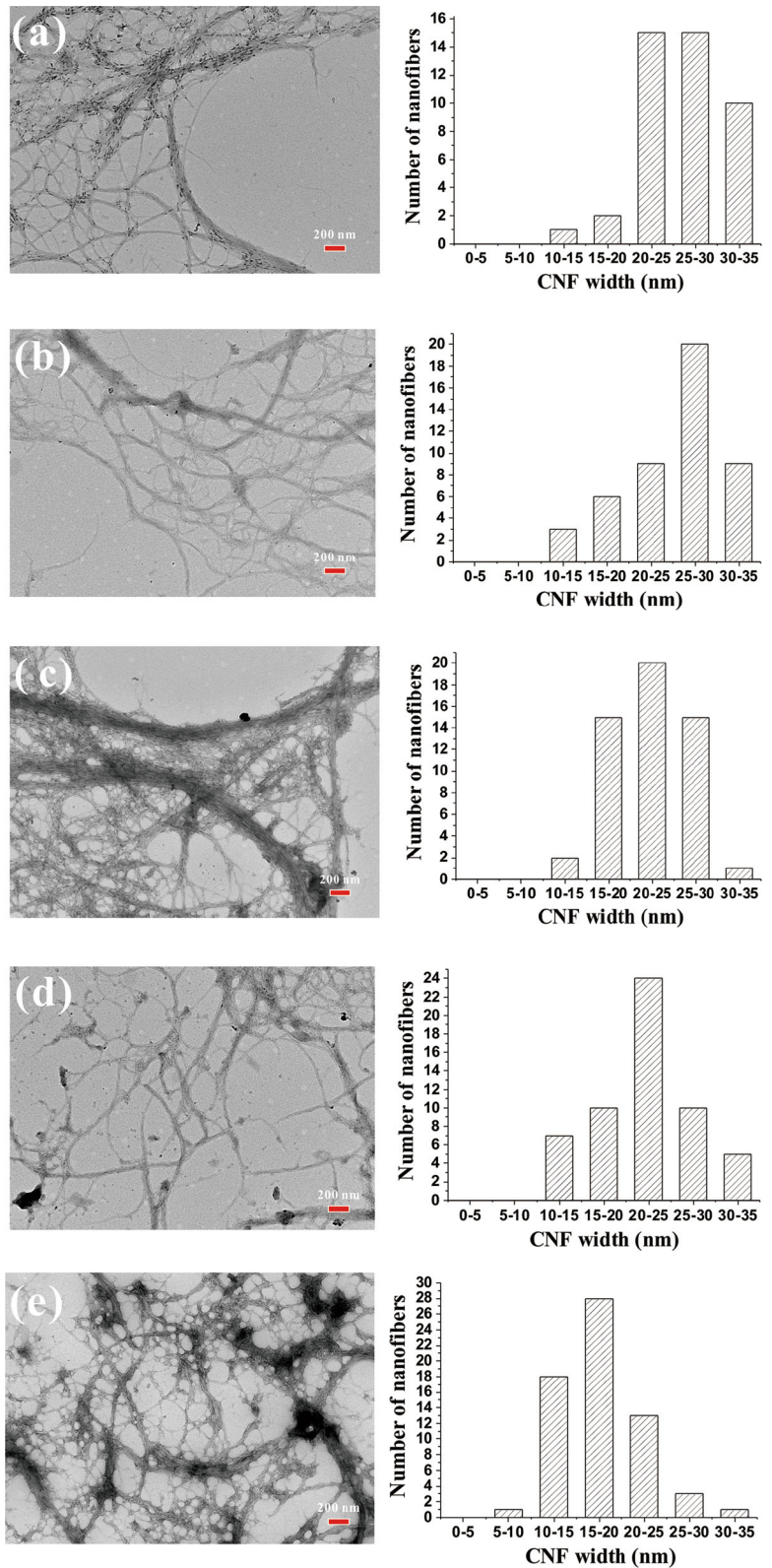
### XRD and FTIR analysis of the CNFs

Figure 3 shows the X-ray diffraction pattern of each CNF sample. It can be seen that all the XRD patterns displayed peaks at  $2\theta = 16.68^\circ$ , and  $22.1^\circ$ , corresponding to the (110), and (200) crystallographic planes, respectively, which are in agreement with the characteristic diffraction peaks of cellulose I $\beta$  (French 2014). This indicated that the crystalline structure of the cellulose fiber will not be changed with different lignin content, and the increase in the lignin content

**Table 1** Properties of the CNF with different amount of lignin

Sample	Cellulose (%)	Klason lignin (%)	Hemicellulose (%)	CNF width (nm)
No-LCNF	77.11±0.60	0.72±0.42	21.77±0.30	26.29±0.61
L-LCNF	71.67±0.42	6.24±0.51	21.68±0.62	25.71±0.44
ML-LCNF	66.1±0.40	11.77±0.24	21.71±0.43	22.21±0.72
MH-LCNF	60.57±0.71	17.29±0.50	21.74±0.80	21.90±0.13
H-LCNF	55.14±0.33	22.81±0.71	21.65±0.24	17.49±0.31

**Fig. 1** TEM of CNF **a** No-LCNF, **b** L-LCNF, **c** ML-LCNF, **d** MH-LCNF, **e** H-LCNF



**Fig. 2** Schematic diagram of lignin scavenging mechanical free radical action

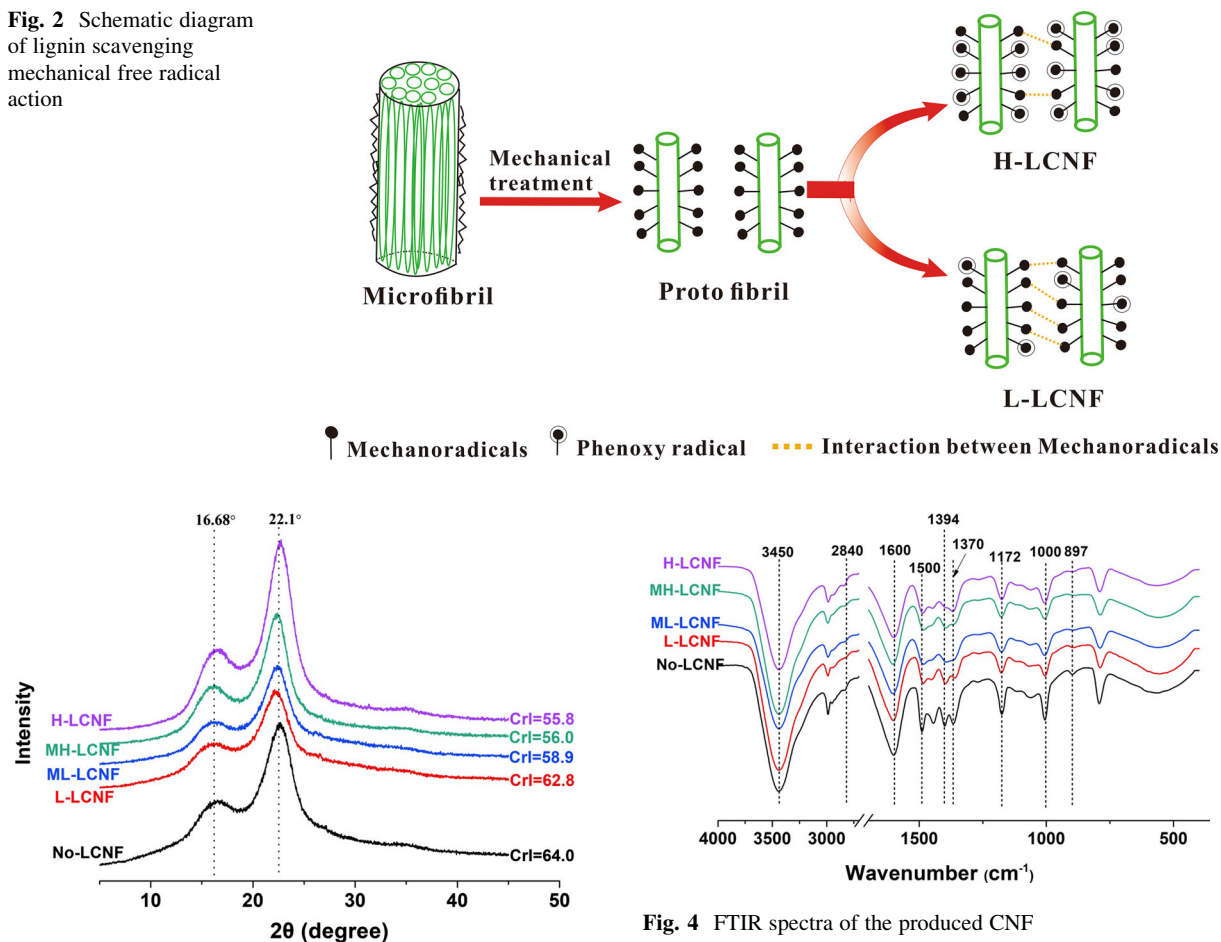


**Fig. 3** X-ray diffraction of CNFs

will not change the crystalline structure of the cellulose fibers. The crystallinity of each CNF sample was calculated by the method of Segal et al (Segal et al. 1959). It can be seen from the crystallization index that as the lignin content in the CNF increases, the crystallinity gradually decreases. H-LCNF has the lowest crystallinity, with a CrI% of 55.8%. No-LCNF has the highest crystallinity, and CrI% was 64%. The crystallinity of H-LCNF was 8.2% lower than that of NO-LCNF, which was mainly due to the increase in the proportion of amorphous regions in the fiber due to the large amount of lignin.

Figure 4 shows an infrared spectrum of each CNF sample at 4000–400  $\text{cm}^{-1}$ . It can be seen from Fig. 4 that the absorption peaks of the CNF samples were basically the same, mainly concentrated in 3500–2800

**Fig. 4** FTIR spectra of the produced CNF

$\text{cm}^{-1}$  and 2000–800  $\text{cm}^{-1}$ . Each CNF sample contains substantially the same functional group, has a distinct absorption peak at 897  $\text{cm}^{-1}$  and did not shift to 895  $\text{cm}^{-1}$ , and showed a type I structural cellulose (Gwon et al. 2010), indicating that the mechanical preparation of CNFs does not change their cellulose crystal structure and functional groups. Detailed analysis shows that there are absorption peaks at 2840, 1600, 1370, and 1172  $\text{cm}^{-1}$ , which are the C-H stretching peaks of lignin (C-H stretching), aromatic ring skeleton vibration absorption peak (aromatic ring vibrations), C-H deformation absorption peak (C-H deformations), guaiacyl benzene ring skeleton absorption peak (guaiacyl ring breathing), and C-O stretching peak (C-O stretching), indicating that each CNF sample contains a certain amount of lignin (Hoareau et al. 2004; Isaac et al. 2018; Nair et al. 2017). The absorption peak at 1500  $\text{cm}^{-1}$  was the characteristic peak of the lignin aromatic skeleton vibration, and this

peak was generated by the shrinkage vibration of the benzene ring C=C bond as a whole. The NO-LCNF sample has a neutral pH of 7, L-LCNF, ML-LCNF, MH-LCNF, and H-LCNF samples have a weak acidic pH of 5-6. Under weakly acidic conditions, the intensity of the absorption peak was weakened and the peak shape was broadened. This was because under the attack of hydroxyl radicals, a ring-opening reaction occurs in the aromatic ring of some electron-rich clouds (Sugimoto et al. 2005). Absorption peaks at 897, 1000, and 1394  $\text{cm}^{-1}$  were related to hemicellulose (Kačuráková et al. 1998; Sun et al. 2004), indicating the presence of hemicellulose in each CNF sample, which is consistent with the conclusions of the CNF sample component analysis, as shown in Table 1.

### Thermal stability of the CNFs

Figure 5 shows a thermogravimetric analysis curve of each CNF sample. According to the variation of mass loss in Fig. 5a, the thermal degradation process of CNF samples can be divided into three regions. Region I was 25 to 206 °C, which was mainly caused by the evaporation of water in each CNF sample to produce a slight mass loss (Zhang et al. 2018c). Region II was 206 °C to 381 °C, which was the main stage of thermal degradation of each CNF sample, and the mass loss was obvious. According to the “Broido-Shafizadeh” cellulose pyrolysis model (Bradbury et al. 1979), cellulose was melted at 200 to 280 °C, and heat was absorbed and dehydrated to form dehydrogenated cellulose. When the temperature

was further increased to 280 to 340 °C, the cellulose underwent a strong depolymerization reaction to form volatiles such as methane, carbon monoxide and carbon dioxide (Isaac et al. 2018).

Taking H-LCNF as an example, the thermal degradation in Region II was analyzed in detail. It can be seen from Fig. 5a that when the heating temperature reached 206 °C, H-LCNF begins to gradually undergo thermal degradation, resulting in slight mass loss. As shown in Table 2, the quality loss of the CNFs at this time was 7.2%. When the temperature was raised to 316 °C, the CNFs experienced a significant mass loss and began to undergo intense thermal degradation. This temperature was defined as the CNF initial thermal degradation temperature ( $T_{\text{onset}}$ ). When the temperature was continuously increased to 363 °C, the CNF mass loss was rapid, and the thermal degradation was the most intense. This temperature was defined as the CNF maximum thermal degradation temperature ( $T_d$ ). When the temperature was further increased to 381 °C, the CNF mass loss again became stable, the thermal degradation also tended to be gradual, and the residual mass was 25.7%. Similarly, thermal degradation analysis of other CNF samples showed that  $T_{\text{onset}}$  and  $T_d$  increased with increasing lignin content in CNF, increasing from 301 °C and 341 °C to 316 °C and 363 °C, respectively. The thermal degradation temperature of Region III ranges from 381 to 600 °C. This region further cracks the thermal degradation intermediates, such as L-glucose produced in Region II to form coke and graphite, which is the

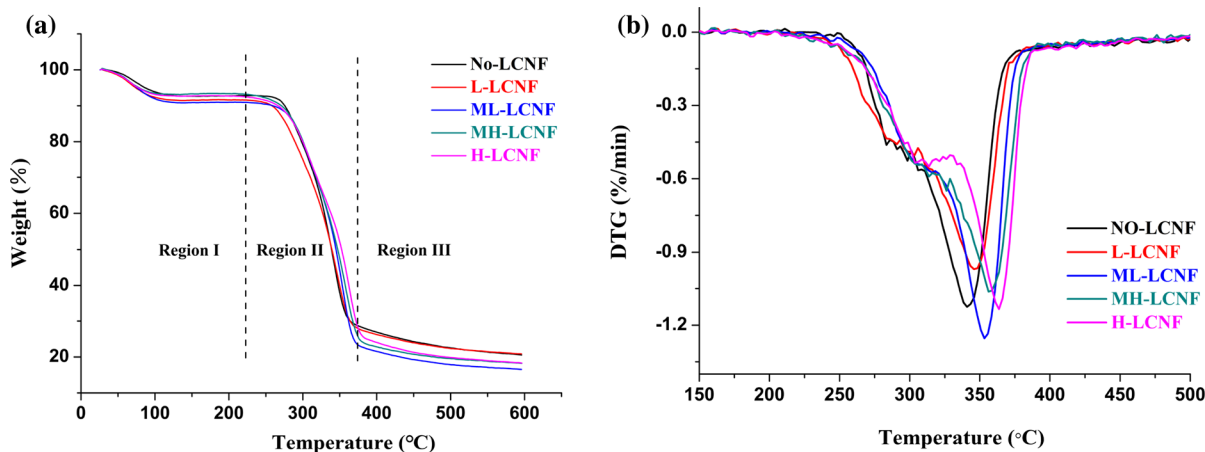


**Fig. 5** TGA (a) and DTG (b) curves of the CNF at a heating rate of 10°/min, from 25° to 600°



**Table 2** Thermal stability of the CNF samples

Sample	Region I		Region II		Region III	T <sub>onset</sub>	T <sub>d</sub>
	Temperature (°C)	Moisture residue (wt%)	Temperature (°C)	Mass residue (wt%)	Mass residue (wt%)		
No-LCNF	233	7.2	366	29.7	20.5	301	341
L-LCNF	216	8.4	368	28.7	20.9	298	346
ML-LCNF	223	9.1	373	23.6	16.5	313	353
MH-LCNF	216	6.7	378	24.5	18.2	308	357
H-LCNF	206	7.2	381	25.7	18.3	316	363

graphitization stage of cellulose (Shafizadeh 1982). At this stage, the thermal degradation of each CNF sample was relatively stable and the mass loss was reduced. The residual mass of each CNF sample at 600 °C was basically the same, approximately 20%; see Table 2 for details.

From the above analysis, it is known that the lignin content in CNFs increased and the crystallinity decreased. The two important indicators reflecting the thermal stability of CNFs, T<sub>onset</sub> and T<sub>d</sub>, showed an increasing trend, which can be explained by the following aspects. The degradation of lignin was less likely to occur below 400 °C. The thermal degradation temperature of cellulose and hemicellulose was generally less than 350 °C. In this stage, the thermal stability of lignin was better than cellulose and hemicellulose (Peng et al. 2018). There were many aromatic groups and different ether carbon bonds in lignin that essentially do not decompose below 300 °C. While cellulose and hemicellulose decompose at lower temperatures, increasing the lignin content of CNFs can increase their thermal stability. Lignin acted as a filler during CNF drying (Rojo et al. 2015) and links to polysaccharides such as cellulose via covalent bonds (Nair et al. 2017; Nair and Yan 2015), making the CNF internal structure more dense, which improved the thermal stability of the CNFs. When CNFs were prepared by TEMPO oxidation, the conclusions obtained were different from those obtained in this study. This was because the TEMPO oxidation process introduces a large number of carboxyl groups with lower thermal stability. When a large number of low thermal stability carboxyl

groups and high thermal stability lignin jointly affect the thermal stability of CNFs, the low thermal stability carboxyl group predominated, and the thermal stability of CNFs overall showed a downward trend. In this work, the high lignin content of CNFs was prepared by a mechanical method using bagasse raw materials without introducing carboxyl groups. Therefore, the lignin content increased in the CNFs and the thermal stability increased.

#### Activation energy of each CNF sample

Figure 6 shows a linear fit of the  $\log \beta$  versus  $1/T$  conversion rate at 20% to 90% using the FWO method to calculate the activation energy of each CNF sample. The linear correlation coefficient was almost 0.999 or more. The relationship between the activation energy and the conversion rate of the thermal decomposition reaction of each CNF sample can be seen in Fig. 7. Because that the point-by-point calculation method was used in this study, cumulative error will inevitably occur. The average of the results obtained thus served as the activation energy for thermal decomposition. The single scan rate method was limited by the choice of reaction mechanism function, and its calculation accuracy was not as accurate as the multiple scan rate method. It can be seen from Fig. 7 that the activation energy of NO-LCNF, L-LCNF, ML-LCNF, MH-LCNF, and H-LCNF were (208.14±16.07), (254.49±16.89), (412.95±11.37), (530.54±39.89), and (652.10±26.27) KJ/mol, respectively. The activation energy of the same CNF sample increases with the increase of the conversion rate. The higher the

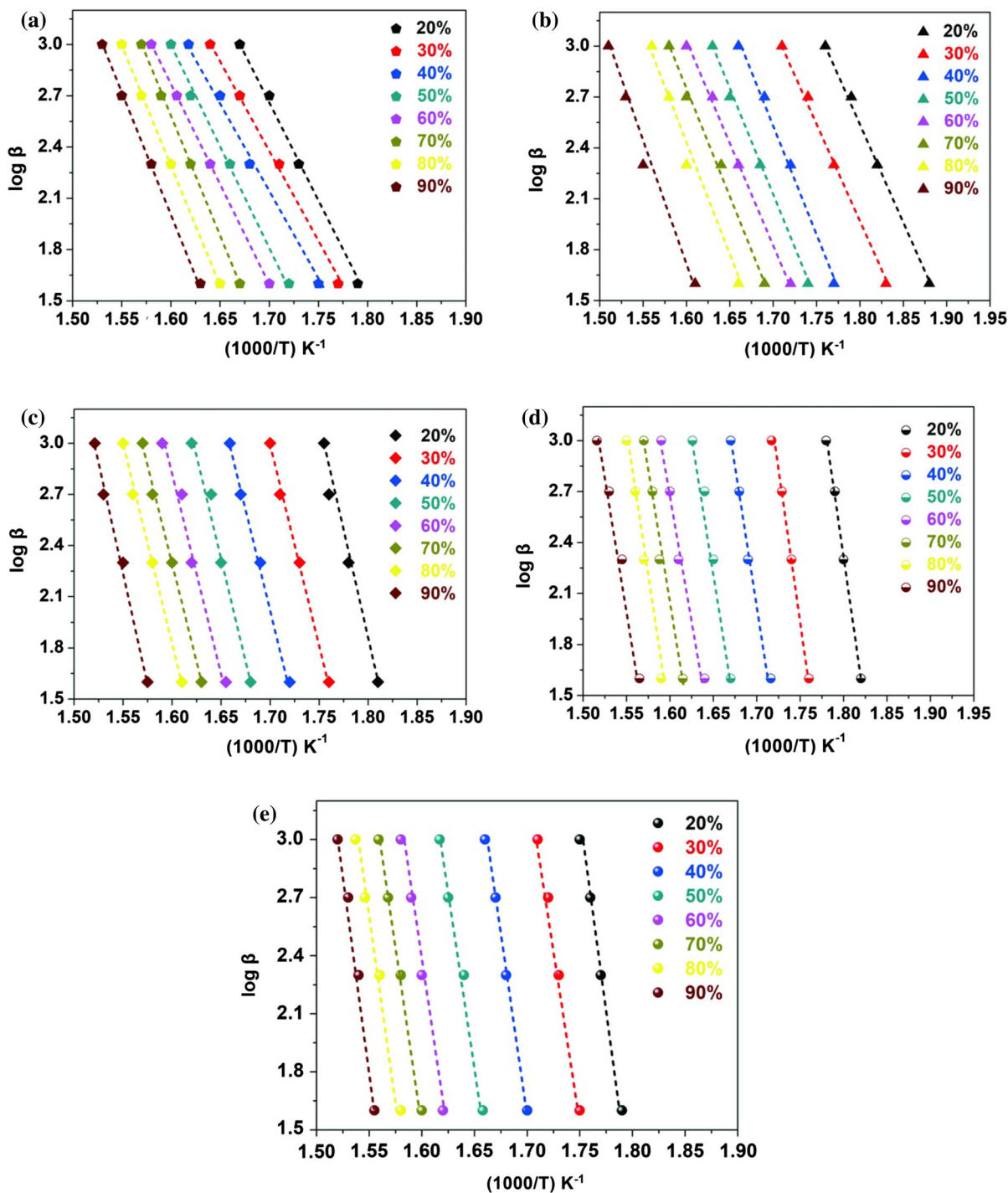


**Fig. 6** Relationship between  $\log \beta$  and  $1/T$  of each CNF sample at different conversion rates ( $\alpha$ ). **a** NO-LCNF; **b** L-LCNF; **c** ML-LCNF; **d** MH-LCNF; **e** H-LCNF

lignin content of the different CNF samples at the same conversion rate, the greater the activation energy value. It indicated that the higher the lignin content of

CNF, the more energy it needed for thermal degradation, and the better its thermal stability, which was consistent with the thermogravimetric analysis. The

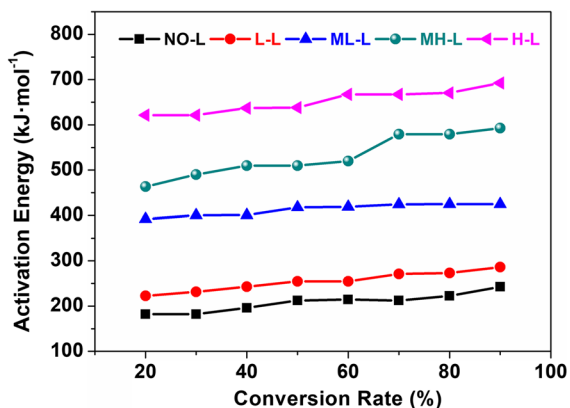


**Fig. 7** Plots for activation energy versus conversion rate for thermal decomposition of different CNF sample

thermal decomposition activation energy of different lignin content CNF calculated was less affected by the conversion rate. As can be seen from Fig. 7, the activation energy of each CNF sample varied with the conversion rate (20%–90%), and the activation energy increases slowly with the increase of conversion rate, indicating that the thermal degradation reaction of each CNF sample in the 30–600 °C stage was similar. When the temperature exceeded 330 °C, the thermal degradation of CNF followed different decomposition mechanisms, and the reaction mechanism become more complicated.

## Conclusions

In this work, CNFs with different lignin contents were prepared by mechanical methods. The thermal stability of CNFs was tested by thermogravimetric analyzer at different heating rates, and the activation energy of CNFs was calculated by FWO method. The results showed that the higher the lignin content in CNF, the better the thermal stability. The thermal decomposition activation energy of CNF fluctuated with the change of conversion rate. Under the same conversion rate, the higher the lignin contents in the sample, the larger the activation energy value. This work provides a theoretical basis for the pyrolysis mechanism and high value utilization of CNFs.

**Acknowledgments** This Project was supported by the National Natural Science Foundation of China (31760192) and the Guangxi Natural Science Foundation of China (2018GXNSFDA281050).

## References

- Alemdar A, Sain M (2008) Isolation and characterization of nanofibers from agricultural residues: wheat straw and soy hulls. *Bioresour Technol* 99:1664–1671. <https://doi.org/10.1016/j.biortech.2007.04.029>
- Bradbury AG, Sakai Y, Shafizadeh F (1979) A kinetic model for pyrolysis of cellulose. *J Appl Polym Sci* 23:3271–3280
- Brown ME, Dollimore D, Galwey AK (1980) Reactions in the solid state, vol 22. Elsevier, Amsterdam
- Chen W, Yu H, Liu Y, Chen P, Zhang M, Hai Y (2011) Individualization of cellulose nanofibers from wood using high-intensity ultrasonication combined with chemical pretreatments. *Carbohydr Polym* 83:1804–1811. <https://doi.org/10.1016/j.carbpol.2010.10.040>
- Dhaundiyal A, Singh SB, Hanon MM, Rawat R (2018) Determination of kinetic parameters for the thermal decomposition of parthenium hysterophorus. *Environ Clim Technol* 22:5–21. <https://doi.org/10.1515/rctect-2018-0001>
- Dong F et al (2019) Sulfadiazine destruction by chlorination in a pilot-scale water distribution system: kinetics, pathway, and bacterial community structure. *J Hazard Mater* 366:88–97
- French AD (2014) Idealized powder diffraction patterns for cellulose polymorphs. *Cellulose* 21:885–896. <https://doi.org/10.1007/s10570-013-0030-4>
- Gwon JG, Lee SY, Doh GH, Kim JH (2010) Characterization of chemically modified wood fibers using FTIR spectroscopy for biocomposites. *J Appl Polym Sci*. <https://doi.org/10.1002/app.31746>
- Hassan M, Berglund L, Hassan E, Abou-Zeid R, Oksman K (2018) Effect of xylanase pretreatment of rice straw unbleached soda and neutral sulfite pulps on isolation of nanofibers and their properties. *Cellulose* 25:2939–2953. <https://doi.org/10.1007/s10570-018-1779-2>
- Hoareau W, Trindade WG, Siegmund B, Castellan A, Frollini E (2004) Sugar cane bagasse and curaua lignins oxidized by chlorine dioxide and reacted with furfuryl alcohol: characterization and stability. *Polym Degrad Stab* 86:567–576. <https://doi.org/10.1016/j.polymdegradstab.2004.07.005>
- Hoeger IC, Nair SS, Ragauskas AJ, Deng Y, Rojas OJ, Zhu JY (2013) Mechanical deconstruction of lignocellulose cell walls and their enzymatic saccharification. *Cellulose* 20:807–818. <https://doi.org/10.1007/s10570-013-9867-9>
- Huang C, He J, Du L, Min D, Yong Q (2016) Structural characterization of the lignins from the green and yellow bamboo of bamboo culm (*Phyllostachys pubescens*). *J Wood Chem Technol* 36:157–172
- Huang C, Dong H, Su Y, Wu Y, Narron R, Yong Q (2019) Synthesis of carbon quantum dot nanoparticles derived from byproducts in bio-refinery process for cell imaging and in vivo bioimaging. *Nanomaterials* 9:387
- Isaac A, de Paula J, Viana CM, Henriques AB, Malachias A, Montoro LA (2018) From nano- to micrometer scale: the role of microwave-assisted acid and alkali pretreatments in the sugarcane biomass structure. *Biotechnol Biofuels* 11:73. <https://doi.org/10.1186/s13068-018-1071-6>
- Kačuráková M, Belton PS, Wilson RH, Hirsch J, Ebringerova A (1998) Hydration properties of xylan-type structures an

- FTIR study of xylooligosaccharides. *J Sci Food Agric* 77:38–44
- Kutsch NP, Gray JR (1970) The potential of lignin research. Maine Agricultural Experiment Station. Technical Bulletin 41
- Li X, Xu R, Yang J, Nie S, Liu D, Liu Y, Si C (2019) Production of 5-hydroxymethylfurfural and levulinic acid from lignocellulosic biomass and catalytic upgradation. *Ind Crops Prod* 130:184–197
- Liao Q et al (2018) Highly cuboid-shaped heterobimetallic metal-organic frameworks derived from porous Co/ZnO/C microrods with improved electromagnetic wave absorption capabilities. *ACS Appl Mater Interfaces* 10:29136–29144. <https://doi.org/10.1021/acsami.8b09093>
- Lin X, Wu Z, Zhang C, Liu S, Nie S (2018) Enzymatic pulping of lignocellulosic biomass. *Ind Crops Prod* 120:16–24. <https://doi.org/10.1016/j.indcrop.2018.04.033>
- Nair SS, Yan N (2015) Effect of high residual lignin on the thermal stability of nanofibrils and its enhanced mechanical performance in aqueous environments. *Cellulose* 22:3137–3150. <https://doi.org/10.1007/s10570-015-0737-5>
- Nair SS, Kuo P-Y, Chen H, Yan N (2017) Investigating the effect of lignin on the mechanical, thermal, and barrier properties of cellulose nanofibril reinforced epoxy composite. *Ind Crops Prod* 100:208–217. <https://doi.org/10.1016/j.indcrop.2017.02.032>
- Nie S et al (2014) Kinetics study of oxidation of the lignin model compounds by chlorine dioxide. *Chem Eng J* 241:410–417. <https://doi.org/10.1016/j.cej.2013.10.068>
- Nie S, Wang S, Qin C, Yao S, Ebonka JF, Song X, Li K (2015) Removal of hexenuronic acid by xylanase to reduce adsorbable organic halides formation in chlorine dioxide bleaching of bagasse pulp. *Bioresour Technol* 196:413–417. <https://doi.org/10.1016/j.biortech.2015.07.115>
- Nie S, Zhang C, Zhang Q, Zhang K, Zhang Y, Tao P, Wang S (2018a) Enzymatic and cold alkaline pretreatments of sugarcane bagasse pulp to produce cellulose nanofibrils using a mechanical method. *Ind Crops Prod* 124:435–441. <https://doi.org/10.1016/j.indcrop.2018.08.033>
- Nie S, Zhang K, Lin X, Zhang C, Yan D, Liang H, Wang S (2018b) Enzymatic pretreatment for the improvement of dispersion and film properties of cellulose nanofibrils. *Carbohydr Polym* 181:1136–1142. <https://doi.org/10.1016/j.carbpol.2017.11.020>
- Pei Y, Wang S, Qin C, Su J, Nie S, Song X (2016) Optimization of laccase-aided chlorine dioxide bleaching of bagasse pulp. *BioResources* 11:696–712
- Peng Y, Nair SS, Chen H, Yan N, Cao J (2018) Effects of lignin content on mechanical and thermal properties of polypropylene composites reinforced with micro particles of spray dried cellulose nanofibrils. *ACS Sustain Chem Eng* 6:11078–11086. <https://doi.org/10.1021/acssuschemeng.8b02544>
- Penttila PA et al (2013) Xylan as limiting factor in enzymatic hydrolysis of nanocellulose. *Bioresour Technol* 129:135–141. <https://doi.org/10.1016/j.biortech.2012.11.017>
- Rojo E, Peresin MS, Sampson WW, Hoeger IC, Vartiainen J, Laine J, Rojas OJ (2015) Comprehensive elucidation of the effect of residual lignin on the physical, barrier, mechanical and surface properties of nanocellulose films. *Green Chem* 17:1853–1866. <https://doi.org/10.1039/c4gc02398f>
- Segal L, Creely JJ, Martin AE, Conrad CM (1959) An empirical method for estimating the degree of crystallinity of native cellulose using the x-ray diffractometer. *Text Res J* 29:786–794
- Shafizadeh F (1982) Introduction to pyrolysis of biomass. *J Anal Appl Pyrol* 3:283–305
- Solala I et al (2012) Mechanoradical formation and its effects on birch kraft pulp during the preparation of nanofibrillated cellulose with Masuko refining. *Holzforchung*. <https://doi.org/10.1515/hf.2011.183>
- Spence KL, Venditti RA, Rojas OJ, Habibi Y, Pawlak JJ (2010) The effect of chemical composition on microfibrillar cellulose films from wood pulps: water interactions and physical properties for packaging applications. *Cellulose* 17:835–848. <https://doi.org/10.1007/s10570-010-9424-8>
- Sugimoto T, Morishita T, Matsumoto Y, Meshitsuka G (2005) Effect of oxygen pressure on the oxidation of syringyl alcohol initiated by manganese(III) acetate. *Holzforchung* 54:262–268
- Sun JX, Sun XF, Sun RC, Su YQ (2004) Fractional extraction and structural characterization of sugarcane bagasse hemicelluloses. *Carbohydr Polym* 56:195–204. <https://doi.org/10.1016/j.carbpol.2004.02.002>
- Tao P, Wu Z, Xing C, Zhang Q, Wei Z, Nie S (2019a) Effect of enzymatic treatment on the thermal stability of cellulose nanofibrils. *Cellulose* 26:1–10
- Tao P, Zhang Y, Wu Z, Liao X, Nie S (2019b) Enzymatic pretreatment for cellulose nanofibrils isolation from bagasse pulp: transition of cellulose crystal structure. *Carbohydr Polym* 214:1–7. <https://doi.org/10.1016/j.carbpol.2019.03.012>
- TAPPI (1992) TAPPI test methods. TAPPI, Peachtree Corners
- Tian X, Lu P, Song X, Nie S, Liu Y, Liu M, Wang Z (2017) Enzyme-assisted mechanical production of microfibrillated cellulose from northern bleached softwood kraft pulp. *Cellulose* 24:3929–3942
- Tynell T, Giri A, Gaskins J, Hopkins PE, Mele P, Miyazaki K, Karppinen M (2014) Efficiently suppressed thermal conductivity in ZnO thin films via periodic introduction of organic layers. *J Mater Chem A* 2:12150–12152
- Wang LW, Fu H, Liu HJ, Yu KF, Wang YH, Ma JM (2018) In-situ packaging ultra-uniform 3D hematite nanotubes by polyaniline and their improved gas sensing properties. *Mater Res Bull* 107:46–53. <https://doi.org/10.1016/j.materresbull.2018.06.034>
- Wu X, Li S, Coumes F, Darcos V, Lai KHJ, Bron P (2013) Modeling and self-assembly behavior of PEG-PLA-PEG triblock copolymers in aqueous solution. *Nanoscale* 5:9010–9017
- Xing J, Tao P, Wu Z, Xing C, Liao X, Nie S (2019) Nanocellulose-graphene composites—a promising nanomaterial for flexible supercapacitors. *Carbohydr Polym* 207:447–459. <https://doi.org/10.1016/j.carbpol.2018.12.010>
- Yao S, Nie S, Yuan Y, Wang S, Qin C (2015) Efficient extraction of bagasse hemicelluloses and characterization of solid remainder. *Bioresour Technol* 185:21–27. <https://doi.org/10.1016/j.biortech.2015.02.052>

- Yao S, Nie S, Zhu H, Wang S, Song X, Qin C (2017) Extraction of hemicellulose by hot water to reduce adsorbable organic halogen formation in chlorine dioxide bleaching of bagasse pulp. *Ind Crops Prod* 96:178–185. <https://doi.org/10.1016/j.indcrop.2016.11.046>
- Yoon B, Lee BH, George SM (2012) Highly conductive and transparent hybrid organic–inorganic zinc oxide thin films using atomic and molecular layer deposition. *J Phys Chem C* 116:24787–24791
- Yu H et al (2018) Enhanced enzymatic hydrolysis of cellulose from waste paper fibers by cationic polymers addition. *Carbohydr Polym* 200:248
- Zhang H, Nie S, Qin C, Zhang K, Wang S (2018a) Effect of hot chlorine dioxide delignification on AOX in bagasse pulp wastewater. *Cellulose* 25:2037–2049. <https://doi.org/10.1007/s10570-018-1670-1>
- Zhang H, Qin C, Nie S, Wang S (2018b) Effects of D-hot pretreatment on micro-distribution of residual lignin in sugarcane bagasse pulp and fiber properties. *Cellulose* 25:4423–4435. <https://doi.org/10.1007/s10570-018-1883-3>
- Zhang K, Zhang Y, Yan D, Zhang C, Nie S (2018c) Enzyme-assisted mechanical production of cellulose nanofibrils: thermal stability. *Cellulose* 25:5049–5061. <https://doi.org/10.1007/s10570-018-1928-7>
- Zhang H, Nie S, Qin C, Wang S (2019a) Removal of hexenuronic acid to reduce AOX formation in hot chlorine dioxide bleaching of bagasse pulp. *Ind Crops Prod* 128:338–345. <https://doi.org/10.1016/j.indcrop.2018.11.025>
- Zhang K, Tao P, Zhang Y, Liao X, Nie S (2019b) Highly thermal conductivity of CNF/AlN hybrid films for thermal management of flexible energy storage devices. *Carbohydr Polym* 213:228–235. <https://doi.org/10.1016/j.carbpol.2019.02.087>
- Zhu H et al (2016) Wood-derived materials for green electronics, biological devices, and energy applications. *Chem Rev* 116:9305–9374. <https://doi.org/10.1021/acs.chemrev.6b00225>

**Publisher's Note** Springer Nature remains neutral with regard to jurisdictional claims in published maps and institutional affiliations.